

## Quantitative study of the decay of intensity oscillations in transient layer-by-layer growth

H.-N. Yang, G.-C. Wang, and T.-M. Lu

*Department of Physics, Applied Physics & Astronomy, Rensselaer Polytechnic Institute, Troy, New York 12180-3590*

(Received 19 September 1994; revised manuscript received 16 February 1995)

An analytical formula for the diffraction from an initial transient layer-by-layer growth front has been derived. The approach utilizes recently developed dynamic scaling models which describe the growth-induced roughening evolution at the late stage of growth. The results can be applied to both out-of-phase and non-out-of-phase diffraction conditions. At the out-of-phase conditions, the Bragg peak intensity is given by  $I_{\text{Bragg}} \propto e^{-\pi^2 w^2} [1 + \cos(2\pi \langle h \rangle)]$ , which oscillates with the growth of the film thickness  $\langle h \rangle$  but decays with the increase of the interface width  $w$  due to the growth-induced roughening. The derived diffraction formula is consistent with the peak intensity oscillation obtained from a transient layer-by-layer process observed in low-temperature molecular-beam epitaxy growth of Si/Si(111).

### I. INTRODUCTION

Growth of crystalline thin films can take place in systems with two phases such as crystal and vapor, crystal and melt, or crystal and solution. A thin film can also be grown by direct deposition of particles on a substrate as in molecular-beam epitaxy (MBE) processes. The study of the growth carried out by techniques such as MBE and metal-organic chemical-vapor deposition (MOCVD) has been a very important topic for both scientific research and industrial applications.

Under near-equilibrium conditions, the growth usually starts with the formation of nuclei. It is well known that the nucleation growth processes can be classified into three conventional types:<sup>1-3</sup> (1) *layer-by-layer growth*, i.e., two-dimensional (2D) nucleation growth [Frank—van der Merwe (FM) mode]; (2) *island growth*, i.e., 3D nucleation growth [Volmer-Weber (VW) mode]; and (3) *layer growth followed by island growth* [Stranski-Krastanov (SK) mode].

The 2D nucleation-dominated growth processes have been observed in many diffraction experiments using techniques such as low-energy electron diffraction (LEED),<sup>4</sup> the reflection high-energy electron diffraction (RHEED),<sup>4</sup> x-ray diffraction,<sup>5</sup> and He-atom diffraction.<sup>6</sup> The layer-by-layer growth manifests itself in the time-dependent oscillation of the measured Bragg peak intensity. Very often, the amplitude of the intensity oscillation decays continuously during growth until it finally vanishes at the later stage of the growth. Two possible mechanisms have been proposed to interpret the transient oscillatory behavior. One is that the damping of the intensity oscillations reflects the emergence of a steady-state (step flow) growth from the 2D nucleation regime without a significant increase of surface roughness. This mechanism is believed to occur at higher growth temperatures. An example has been shown in the MBE growth of GaAs film on a GaAs(001) surface at 555 °C.<sup>7</sup> Another mechanism is suggested to occur at lower growth temperatures, where, due to the low atomic mobility, the diffusion is unable to compete with the growth-induced fluctuation. Therefore, a steady-state step structure is

unlikely to occur. Under this circumstance, the decay of intensity oscillations is likely an indication of the occurrence of kinetic roughening below the equilibrium roughening transition temperature. In this paper, we shall focus on the topic of the roughening-induced transient layer-by-layer growth.

It was shown by Saarloos and Gilmer in their polynuclear growth (PNG) model<sup>8</sup> that if multiple nucleation events occur in layer growth at a sufficiently high nucleation rate, the global interface can grow into a dynamic roughening morphology which resembles the simple random-walk picture. Thus, as far as the nonequilibrium dynamics is concerned, even the 2D nucleation-dominated growth could eventually evolve into a multilevel rough surface. The roughening evolution can be described by stochastic Langevin equations which include kinetic effects, the random fluctuation, and the relaxation mechanism. Two kinds of stochastic Langevin models have been proposed: one considers growth conditions dominated by the evaporation-condensation processes;<sup>9-12</sup> another one describes growth processes which proceed with the deposition and atomic diffusion but without desorption.<sup>13-21</sup> Both models can predict the existence of an initial layer-by-layer growth process. The growth-induced roughening will finally evolve into a region where the morphology shows a dynamic scaling behavior.<sup>22</sup>

Roughening-induced transient layer-by-layer phenomena were studied previously using various microscopic (lattice) models.<sup>3,23-34</sup> A modified Eden model simulation<sup>28</sup> showed that at the initial growth stage, the interface width which measures the surface roughness oscillates itself, and the scaling properties of kinetic roughening can only be observed once these oscillations are damped out. Such an initially nonmonotonous change of the interface width originates from the intrinsic substrate effect where holes, overhangs, and multiple steps are not allowed, so that the morphology cannot become rough quickly at the beginning stage of growth. However, a recent simulation<sup>34</sup> indicated that an effective scaling can occur even in the early growth regime, and that the Bragg intensity oscillations tend to decay as  $e^{-0.99w^2}$ ,

where  $w$  denotes the interface width. This implies that under circumstances where the intrinsic substrate effect is less influential, so that the oscillation of interface width is negligibly small, then the dynamic scaling properties can be observed in the early stage of growth. One such example is the low-temperature MBE growth of materials with strong chemical bonding (such as Si), where multiple steps might be created due to the slow atomic mobility and fast deposition. In this paper, we present a quantitative study of diffraction characteristics from a roughening-induced transient layer-by-layer growth front. Considering the cases where intrinsic substrate effect is at a minimum, we have derived analytical form for the damped Bragg intensity oscillation based on the growth dynamics described by stochastic Langevin models. Detailed discussion of these models is given in Sec. II, and the derivation of the decay in intensity oscillation is presented in Sec. IV. In Sec. V, we give an example of the low-temperature MBE growth of Si/Si(111). In addition, in Sec. III we show the diffraction characteristics for an ideal layer-by-layer growth front. The study is expected to provide a useful analytical tool for the diffraction study of layer-by-layer growth phenomenon.

## II. GROWTH DYNAMICS: STOCHASTIC LANGEVIN MODELS

### A. Growth with surface tension: Evaporation, condensation and 2D nucleation

A phenomenological Langevin equation that incorporates the processes of evaporation, condensation, and 2D nucleation has been proposed as<sup>9-12</sup>

$$\frac{\partial}{\partial t} z(\mathbf{r}, t) = \nu \nabla^2 Z(\mathbf{r}, t) + D \Delta \mu / T + \eta(\mathbf{r}, t) - V \sin \left[ \frac{2\pi Z(\mathbf{r}, t)}{c} \right], \quad (1)$$

where  $\mathbf{r} = (x, y)$  is the positional vector along surface, and  $Z(\mathbf{r}, t)$  represents the surface height of the position  $\mathbf{r}$  at the growth time  $t$ . Equation (1) is a Sine-Gorden equation. The first term on the right-hand side of the equation describes the relaxation driven by surface tension via evaporation and condensation processes, where the coefficient  $\nu$  is the surface tension. The second term is related to the nucleation driving force for crystal growth, where  $\Delta \mu$  is the chemical potential difference between the crystal phase and the vapor phase. The term  $D \Delta \mu / T$  actually represents the deposition rate (impinging rate) of atoms from vapor onto a crystal surface.  $\eta(\mathbf{r}, t)$  is the noise simulating random fluctuations that induce the roughening during growth.  $\eta(\mathbf{r}, t)$ 's are independent Gaussian random variables which satisfy the statistical relation

$$\langle \eta(\mathbf{r}, t) \rangle = 0, \quad (2)$$

$$\langle \eta(\mathbf{r}, t) \eta(\mathbf{r}', t') \rangle = 2D \delta(\mathbf{r} - \mathbf{r}') \delta(t - t'),$$

where  $D$  is the mean square amplitude of the noise. The fourth term,  $V \sin[2\pi Z(\mathbf{r}, t)/c]$ , is the pinning force for a

crystalline surface, which energetically favors integer values of heights,  $Z(\mathbf{r}, t)$ , in units of the layer spacing  $c$ .  $V$  is the amplitude of the pinning force.

The physics implicated in Eq. (1) can be understood from the following qualitative analysis. After taking a statistical average on each term in Eq. (1), and based on the fact that  $\langle \nabla^2 Z(\mathbf{r}, t) \rangle = 0$ , we obtain a growth rate equation

$$\frac{\partial}{\partial t} \langle Z(t) \rangle = D \Delta \mu / T - V \left\langle \sin \left[ \frac{2\pi Z(\mathbf{r}, t)}{c} \right] \right\rangle. \quad (3)$$

One may notice that the term  $\partial/\partial t \langle Z(t) \rangle$ , which represents the actual growth rate, is not equal to the impinging rate of deposition,  $D \Delta \mu / T$ , because of the contribution from the pinning force,  $V_{\text{pinning}} = -V \langle \sin[2\pi Z(\mathbf{r}, t)/c] \rangle$ . The contribution from  $V_{\text{pinning}}$  can originate from the evaporation and recondensation processes. In a layer-by-layer growth process, a majority of atoms and islands are in the top layer of the surface. The average surface height (film thickness) can be approximately expressed as  $\langle Z(t) \rangle = (m + \theta)c$ , where  $m$  is the integral part of the film thickness and  $\theta$  is the coverage of deposited atoms in the top layer. For the purpose of discussion, we can roughly replace  $Z(\mathbf{r}, t)$  by  $\langle Z(t) \rangle$  in the pinning force,  $V_{\text{pinning}} \approx -V \sin[2\pi \langle Z(t) \rangle / c] = -V \sin(2\pi \theta)$ . As shown in Fig. 1,  $V_{\text{pinning}}$  is negative between  $\theta = 0$  and  $0.5$  (half-monolayer) and then positive from  $\theta = 0.5$  to  $\theta = 1$  (1 ML). The negative  $V_{\text{pinning}}$  indicates the occurrence of desorption (evaporation) events, while positive  $V_{\text{pinning}}$  implies the recondensation.

The behavior of the pinning force reflects qualitatively the reality of the 2D nucleation-dominated growth process. At  $\theta \leq 0.25$ , since few atoms exist in the top layer, the probability that 2D clusters overcome the potential barrier to reach the critical nuclei size is small. Therefore, a number of deposited atoms which are not stable in the crystal surface will evaporate onto the vapor phase.

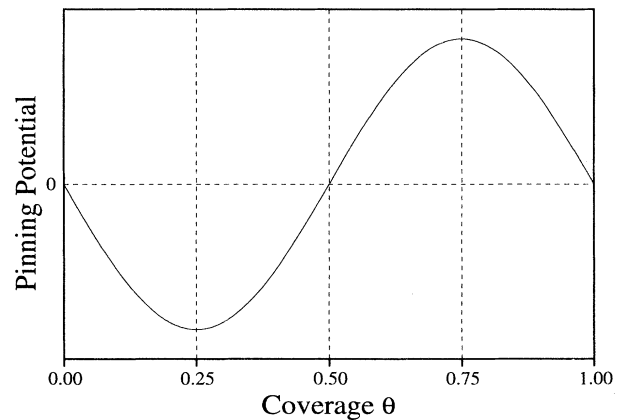


FIG. 1. The pinning force  $V_{\text{pinning}} \approx -V \sin[2\pi \langle Z(t) \rangle / c]$  is plotted as a function of the coverage for deposited atoms in the top layer. The behavior of  $V_{\text{pinning}}$  reflects qualitatively the reality of the 2D nucleation-dominated growth process.

$V_{\text{pinning}}$  thus makes an increasing negative contribution to the growth rate, as shown in Fig. 1 between  $\theta=0$  and 0.25. With the increase of the coverage, the probability for 2D nuclei to reach the critical nuclei size increases. As a result, the negative pinning potential starts to decrease, as shown between  $\theta=0.25$  and 0.5 in Fig. 1. When the coverage further increases, the top layer contains so many atoms that the growth is much easier.  $V_{\text{pinning}}$  thus becomes increasingly positive and the condensation processes are dominant at  $0.5 \leq \theta \leq 0.75$ . Beyond  $\theta=0.75$ , the positive pinning force starts to decrease until  $\theta=1$ . The reason for the decrease may be due to the lack of nucleation events in a new layer, which slows down the growth process.

It is shown that Eq. (1) captures the essential physics in the growth processes which involve evaporation, condensation, and 2D nucleation. This model exhibits a nonconservative dynamics because the sticking coefficient of deposition atoms is less than 1 due to evaporation. Renormalization-group (RG) analysis<sup>11,12</sup> of Eq. (1) further indicates that the growth morphology depends strongly on the chemical potential driving force,  $D\Delta\mu/T$ . The dynamics can be classified into two categories.

### 1. Small driving force: Near equilibrium dynamics

For a very small chemical potential difference,  $\Delta\mu \sim 0$ , the growth proceeds in near-equilibrium dynamics. The corresponding morphology is similar to that on an equilibrium surface. Below the equilibrium roughening transition temperature  $T_R$ , the pinning force is dominant and the surface forms a flat phase, where the growth occurs via ideal layer-by-layer nucleation. At  $T < T_R$ , the growth rate  $R \sim 0$ ,<sup>9</sup> which, to the first order, is consistent with the general form of nucleation growth rate,  $R \sim e^{-D_0/\Delta\mu}$ , where  $D_0$  depends on temperature. In contrast to the low-temperature growth, at high temperatures above  $T_R$  the surface will remain rough during growth. In analog to the equilibrium case, the dynamic phase transition<sup>9,11,12</sup> of the growth morphology near  $T_R$  is of the Kosterlitz-Thouless (KT) type.<sup>35</sup> We must emphasize that the flat phase discussed here is only meaningful for certain length scale [such as the length scales measured in scanning tunneling microscopy (STM) or the correlation lengths in diffraction techniques]. On sufficiently large scales, the growing surface could become rough no matter how strong the driving force is. Therefore, we keep in mind that the flat phase discussed in this paper should always refer to a limited length scale.

### 2. Large driving force: Far-from-equilibrium processes

In the presence of a finite chemical potential difference, the large driving force can lead to a far-from-equilibrium dynamics where the growth-induced roughening occurs below  $T_R$ . Such a dynamic roughening is consistent with the prediction from the PNG model.<sup>8</sup> As pointed out by Nozières,<sup>12</sup> the growth under a large driving force can be compared with the thermodynamics of a vicinal surface where the equilibrium roughening transition takes place below  $T_R$ . A sufficiently large driving force is equivalent

to a large tilt angle of a vicinal surface, which blurs the KT roughening transition and washes out the pinning force to zero. In the absence of the pinning force, Eq. (1) becomes an Edwards-Wilkinson model<sup>10</sup> that describes a far-from-equilibrium growth dynamics where the morphology undergoes both vertical roughing and lateral coarsening evolution.

The vertical roughness can be characterized by the root-mean-square height fluctuation, i.e., the interface width  $w = \sqrt{\langle [Z(\mathbf{r}, t) - \langle Z(t) \rangle]^2 \rangle}$ , where  $\langle Z(t) \rangle$  is the average surface height (or film thickness) at growth time  $t$ . The lateral coarsening can be described by a lateral correlation length  $\xi$ , a distance within which the surface height fluctuations are correlated but beyond which the variations spread and are not correlated. For the Edwards-Wilkinson model, shown as Eq. (1) with  $V=0$ , the lateral correlation length is found to grow with time as  $\xi = \sqrt{2\nu t}$  and the interface width is given by (cf. Appendix A)

$$w^2 \sim \int_0^{1/b_c} dq \frac{1 - e^{-2\nu q^2}}{q} \approx \ln(1 + t/\tau_c), \quad (4)$$

where  $b_c$  is the short length-scale cutoff (with an order of the lattice constant), and  $\tau_c$  is a time constant  $\tau_c^{-1} = 2\nu/b_c^2$ . The surface height distribution can be shown rigorously (see Appendix A) to give a Gaussian-type function:

$$\rho(Z) = \frac{1}{\sqrt{2\pi}w} \exp\left\{-\frac{[Z - \langle Z(t) \rangle]^2}{2w^2}\right\}. \quad (5)$$

In addition, one can obtain analytically the height-height correlation function, which is a measure of the relative height fluctuation in a surface:<sup>10</sup>

$$\begin{aligned} & \langle [Z(\mathbf{r}, t) - Z(0, t)]^2 \rangle \\ & \sim \int_0^{1/b_c} dq [1 - J_0(qr)] \frac{1 - e^{-2\nu q^2}}{q} \\ & \sim \begin{cases} \ln(r) & \text{for } r \ll \xi \\ \ln(t) & \text{for } r \gg \xi, \end{cases} \end{aligned} \quad (6)$$

where  $J_0(x)$  is the zeroth-order Bessel function.

We should point out that the expressions in Eqs. (4) and (6) agree with general dynamic scaling forms:  $w \sim t^\beta$  and  $\langle [h(\mathbf{r}) - h(0)]^2 \rangle = 2w^2 f(r/\xi)$ , where the scaling function  $f(x) = 1$ , for  $x \gg 1$ , and  $f(x) = x^{2\alpha}$ , for  $x \ll 1$ .  $\alpha$  is the roughness exponent which describes the local surface roughness. The exponent  $\beta$  is related to the growth process. The dynamic scaling approach<sup>22</sup> is a very useful tool for describing the evolution of growth fronts. For the present Edwards-Wilkinson dynamics,  $\alpha = \beta = 0$ . Experimental evidence of this growth dynamics has been reported recently in two growth cases.<sup>36,37</sup>

### B. Growth with surface diffusion: Conservative MBE growth dynamics

In one type of MBE processes, such as in Si epitaxial growth, the primary relaxation mechanism is atomic diffusion, where the deposited atoms can relax to the

nearest kink or proceed to site-to-site hopping. The diffusion relaxation is temperature dependent and follows an Arrhenius behavior. Since the deposited atoms are chemisorbed to saturate the strong chemical bonds in the substrate, the surface tension type of relaxation via the evaporation and recondensation process is negligible. Therefore, this type of MBE process must be governed by a mass conservative dynamics, which is in contrast to the nonconservative model discussed in Sec. II A. Incorporating all these important characteristics, a Langevin equation for conservative MBE growth processes has been proposed as<sup>13-17</sup>

$$\frac{\partial}{\partial t} Z(\mathbf{r}, t) = R - \kappa \nabla^4 Z(\mathbf{r}, t) + \eta(\mathbf{r}, t) - V \nabla^2 \sin \left[ \frac{2\pi Z(\mathbf{r}, t)}{c} \right], \quad (7)$$

where  $R$  is the impinging rate from a MBE source. The  $\nabla^4$  term represents the local diffusion, and  $\kappa$  is the diffusion coefficient governed by the Arrhenius law,  $\kappa \sim e^{-E_a/k_B T}$ , where  $E_a$  is the activation energy for nearest-neighbor hopping. Note that the  $\nabla^2$  term which represents the surface tension in Eq. (1) is absent in Eq. (7). We should point out that generically this Laplacian term should be present due to the nonequilibrium statistics of surface configurations.<sup>38</sup> Compared with the  $\nabla^4$  term, the  $\nabla^2$  term makes a more significant contribution in longer time and larger length scale. We are more interested in the earlier stage and shorter length scale where the diffusion is the dominant smoothing mechanism. Therefore, for simplicity, at the present time we are not considering the contribution from the  $\nabla^2$  term. Besides, as a consequence of the conservation law, the form of the pinning force,<sup>15</sup>  $-V \nabla^2 \sin[2\pi Z(\mathbf{r}, t)/c]$ , is different from that for the nonconservative growth shown in Eq. (1). Since for any function of  $F(\mathbf{r})$ ,  $\langle \nabla^2 F(\mathbf{r}) \rangle = 0$ , we can easily show from Eq. (7) that the growth rate  $\partial/\partial t \langle Z(\mathbf{r}, t) \rangle$  is exactly equal to the impinging rate of  $R$ . This is consistent with the conservative dynamics in conservative MBE processes.

Renormalization analysis<sup>15</sup> of Eq. (7) indicates that two different morphologies can be produced during growth, i.e., a high-temperature flat phase and a low-temperature nonequilibrium rough phase. The temperature-dependent diffusion coefficient  $\kappa$  is solely responsible for such a phase change. At high temperatures (below  $T_R$ ), the pinning force combined with a large  $\kappa$  leads to a flat phase, which gives a model for the ideal layer-by-layer growth. However, at low temperatures, the pinning force is renormalized to zero. In the absence of the pinning force, Eq. (7) becomes a Wolf-Villain model that describes the far-from-equilibrium dynamics undergoing both vertical roughening and lateral coarsening evolution.<sup>13-21</sup> This temperature-dependent behavior in MBE growth is just opposite to that predicted from Eq. (1) for the surface-tension growth model where a surface is flat at low temperatures but is rough at high temperatures (see Sec. II A). Nevertheless, both predictions for the temperature-dependent growth are supported by recent experimental observations from different growth systems.

For example, the temperature-dependent behavior in the growth of He on <sup>4</sup>He(0001) facet<sup>36</sup> is more consistent with the surface-tension model shown by Eq. (1). On the other hand, the temperature-dependent growth of Si/Si(111) (Ref. 39) agrees with the conservative MBE dynamics given by Eq. (7). It is understandable, that for the MBE growth, the fast atomic diffusion at high temperatures is able to smooth the fluctuation, while at low temperature the diffusion is so slow that the fluctuation prevails to produce a rough phase. Equation (7) thus captures the essential physics in MBE processes.

For the Wolf-Villain model, shown as Eq. (7) with  $V=0$ , dynamic scaling laws can be derived<sup>13-21</sup> to give a lateral correlation length,  $\xi = (2\kappa t)^{1/4}$  and an interface width (cf. Appendix A)

$$w^2 \sim \int_0^{1/b_c} dq \frac{1 - e^{-2\kappa t q^4}}{q^3} \sim t^{1/2}. \quad (8)$$

Again, the surface height distribution function is found to be identical to Eq. (5), i.e., a Gaussian distribution (see Appendix A). The height-height correlation function from Eq. (7) with  $V=0$  can be calculated as<sup>18</sup>

$$\begin{aligned} & \langle [Z(\mathbf{r}, t) - Z(0, t)]^2 \rangle \\ & \sim \int_0^{1/b_c} dq [1 - J_0(qr)] \frac{1 - e^{-2\kappa t q^4}}{q^3} \\ & \sim \begin{cases} r^2 \ln(t/r^4) & \text{for } r \ll \xi \\ t^{1/2} & \text{for } r \gg \xi \end{cases}. \end{aligned} \quad (9)$$

The growth-induced roughening in a conservative MBE growth is distinctly different from that in the surface-tension model. For MBE growth,  $\alpha=1$  and  $\beta=\frac{1}{4}$ , while for the surface-tension model  $\alpha=\beta=0$ . They belong to different classes of dynamics. [The conservative MBE growth dynamics has been observed recently in the growth of Si/Si(111) (Ref. 39). We shall show below that different time-dependent interface widths  $w \sim t^{1/4}$  (MBE model) and  $w \sim \sqrt{\ln(t)}$  (surface-tension model), manifest themselves in the decay of Bragg intensity oscillations in the region of transient layer-by-layer growth.

### III. DIFFRACTION FROM AN IDEAL LAYER-BY-LAYER GROWTH FRONT

Under appropriate deposition conditions, both growth models discussed in Sec. II predict the existence of an ideal layer-by-layer growth process in which the surface contains steps that are confined within top two levels. The distribution of steps can be completely random<sup>40-44</sup> or partially correlated.<sup>45-48</sup> In the present study, we shall consider only a random distribution of steps in two-level systems.

#### A. Height difference function and height-height correlation function

The height difference function is defined as  $C(\phi, \mathbf{r}) = \langle e^{i\phi[h(\mathbf{r}) - h(0)]} \rangle$ , where  $\phi$  is a phase constant related to the diffraction condition.  $h(\mathbf{r}) = Z(\mathbf{r}, t)/c$  represents the surface height in units of  $c$ .  $C(\phi, \mathbf{r})$  de-

scribes the statistical average of the phase difference between two points in a surface. Under the two-level restriction and the assumption of randomly distributed steps, the expression for the height difference function has been shown to have the following form:<sup>44</sup>

$$\begin{aligned} C(\phi, \mathbf{r}) &= \cos^2(\phi/2) + \sin^2(\phi/2)C(\phi = \pi, \mathbf{r}) \\ &= 4\theta(1-\theta)\sin^2(\phi/2)e^{-r/\xi} \\ &\quad + [1 - 4\theta(1-\theta)\sin^2(\phi/2)], \end{aligned} \quad (10)$$

where  $C(\phi = \pi, \mathbf{r})$  is given by den Nijs and Rommelse<sup>42</sup> as

$$C(\phi = \pi, \mathbf{r}) \sim C_0 e^{-r/\xi + \rho^2}, \quad (11)$$

with  $\rho^2 = (1-2\theta)^2$  and  $C_0 = 4\theta(1-\theta)$ .

In Eq. (10), the constant term  $[1 - 4\theta(1-\theta)\sin^2(\phi/2)]$  reflect long-range order while the exponential function  $e^{-r/\xi}$  exhibits a short-range disorder. This type of random distribution of steps can occur in many physical systems, including an equilibrium surface structure below the roughening transition temperature.<sup>43</sup> For the present layer-by-layer growth problem, the correlation length  $\xi$  is interpreted as the average size of 2D clusters.

The corresponding height-height correlation can be simply calculated from Eq. (10) as

$$\begin{aligned} \langle [h(\mathbf{r}) - h(0)]^2 \rangle &= -\frac{d^2}{d\phi^2} \langle e^{i\phi[h(\mathbf{r}) - h(0)]} \rangle \Big|_{\phi=0} \\ &= 2\theta(1-\theta)(1 - e^{-r/\xi}). \end{aligned} \quad (12)$$

The interface width  $w$  can then be obtained as

$$w/c = \lim_{r \rightarrow \infty} \sqrt{\frac{1}{2} \langle [h(\mathbf{r}) - h(0)]^2 \rangle} = \sqrt{\theta(1-\theta)}.$$

Since  $0 \leq \theta \leq 1$ ,  $w/c = \sqrt{\theta(1-\theta)} \leq [\theta + (1-\theta)]/2 = \frac{1}{2}$ . Thus the thickness of the crystal-vapor interface,  $2w$ , will not exceed the layer spacing  $c$  during layer-by-layer growth.

### B. Diffraction intensity from an ideal layer-by-layer growth front

The diffraction structure factor  $S(\mathbf{k}_{\parallel}, k_{\perp})$ , which is proportional to the diffraction intensity, represents the Fourier transform of the height difference function,

$$S(\mathbf{k}_{\parallel}, k_{\perp}) = \int d\mathbf{r} C(\phi, \mathbf{r}) e^{i(\mathbf{k}_{\parallel} - \mathbf{G}_{hk}) \cdot \mathbf{r}}, \quad (13)$$

where  $\mathbf{G}_{hk}$  represents the Bragg lattice vectors in a 2D surface, and  $\mathbf{k}_{\parallel}$  and  $k_{\perp}$  are diffraction momentum transfers parallel and perpendicular to the surface, respectively. The phase constant  $\phi$  is determined by  $\phi = k_{\perp}c$ .  $\phi = (2n+1)\pi$ ,  $n=0, 1, 2, \dots$ , is the out-of-phase condition at which destructive interference occurs between the diffract ion from different surface layers.  $\phi = 2n\pi$  is the in-phase condition at which constructive interference occurs.

To study the diffraction from an ideal layer-by-layer growth front, we insert Eq. (10) into Eq. (13). The diffraction structure factor is obtained as<sup>44</sup>

$$\begin{aligned} S(\mathbf{k}_{\parallel}, k_{\perp}) &\sim 4\theta(1-\theta)\sin^2(\phi/2)L_2 \left[ \frac{\mathbf{k}_{\parallel} - \mathbf{G}_{hk}}{\sigma_L} \right] \\ &\quad + [1 - 4\theta(1-\theta)\sin^2(\phi/2)]\delta(\mathbf{k}_{\parallel} - \mathbf{G}_{hk}), \end{aligned} \quad (14)$$

where  $\sigma_L = \xi^{-1}$  and  $L_2(x)$  is the 2D Lorentzian function given by  $L_2(x) \propto (1+x^2)^{-3/2}$ .

In Eq. (14), the diffraction intensity distribution has a form of  $\delta + L_2$ , i.e., a sharp  $\delta$  peak (Bragg peak) superimposed on a broad Lorentzian line shape. The full width at half maximum (FWHM) of the Lorentzian shape is inversely proportional to the average size of 2D clusters,  $\text{FWHM} = 2\sigma_L \sqrt{2^{2/3} - 1} \approx 1.53\xi^{-1}$ . To show the  $\delta + L_2$  type of line shape, in Fig. 2 we plot Eq. (14) at  $\phi = 2\pi$  (in-phase condition),  $\phi = 0.5\pi$ , and  $\phi = \pi$  (out-of-phase condition), respectively. Here  $\theta$  is assumed to be a half-monolayer coverage and the  $\delta$  function is convoluted with a Gaussian function which represents an instrument response.

Since  $\langle h \rangle = m + \theta$ , the diffraction demonstrates an undamped oscillatory Bragg intensity,  $I_{\text{Bragg}} \propto 1 - 4\theta(1-\theta)\sin^2(\phi/2)$ , as a function of the film thickness,  $\langle h \rangle$ , as shown in Fig. 3(a). At out-of-phase diffraction conditions,  $\phi = (2n+1)\pi$ ,  $I_{\text{Bragg}} \propto (2-\theta)^2$ , which has a maximal oscillation amplitude due to the destructive interference of the diffraction scattered from the first and second layers in a surface. The oscillation also exists in the diffuse Lorentzian intensity  $[\propto \theta(1-\theta)\sin^2(\phi/2)]$ , as plotted in Fig. 3(b). As shown in Fig. 2, at the half-monolayer coverages  $\langle h \rangle = m + \frac{1}{2}$ ,

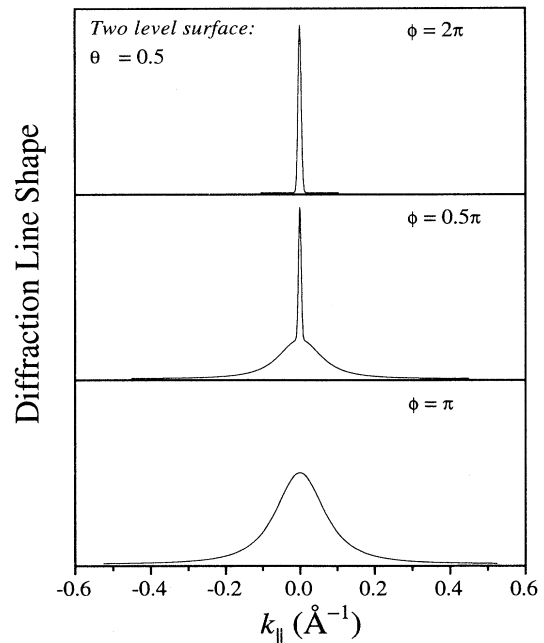


FIG. 2. Diffraction line shapes from a two-level surface at  $\phi = 2\pi$  (in-phase condition),  $\phi = 0.5\pi$ , and  $\phi = \pi$  (out-of-phase condition), where  $\theta$  is assumed to be a half-monolayer coverage. The line shape at  $\phi = 0.5\pi$  shows a sharp  $\delta$  peak superimposed on a broad 2D Lorentzian diffuse profile. At  $\phi = \pi$ , the  $\delta$  peak vanishes, while, at  $\phi = 2\pi$ , the diffuse line shape disappears.

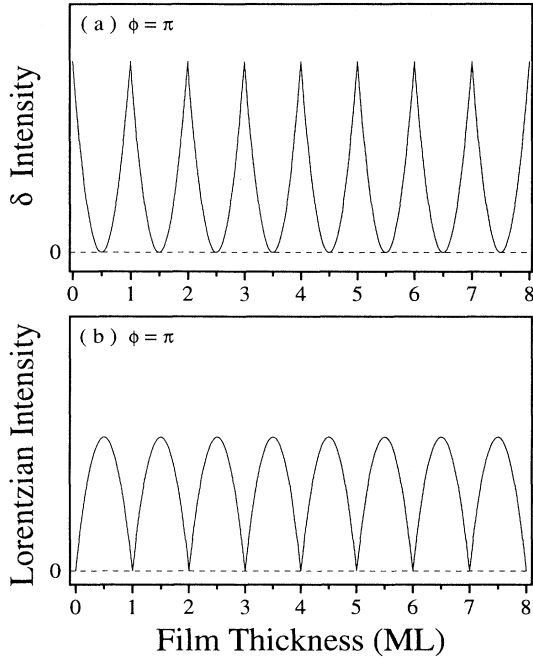


FIG. 3. The central  $\int$  intensity and the diffuse Lorentzian intensity from a two-level surface are plotted as a function of the film thickness in (a) and (b), respectively. The diffraction condition is at  $\phi = \pi$ , i.e., an out-of-phase condition.

the Bragg intensity vanishes while the diffuse intensity reaches a maximum as a result of destructive interference. At integer monolayer coverages  $\langle h \rangle = m$ , where the surface is completely flat, the Bragg intensity reaches a maximum while the diffuse profile vanishes. However, the Bragg intensity does not oscillate with  $\langle h \rangle$  at in-phase diffraction conditions,  $\phi = 2n\pi$ , due to the constructive interference. Note that similar results were obtained also from a 1D two-level model.<sup>40,41</sup>

#### IV. DIFFRACTION FROM TRANSIENT LAYER-BY-LAYER GROWTH FRONT

As shown in Sec. II, the growth-induced roughening can take place under far-from-equilibrium conditions after the pinning potential is renormalized to zero. After a sufficiently long time, i.e., at the late stage of growth, the roughening evolution exhibits dynamic scaling behaviors, as shown in Eqs. (4) and (6) for a surface-tension model and in Eqs. (8) and (9) for a MBE model, respectively. However, since film growth processes usually start from a flat substrate surface, the pinning potential cannot be washed out at the initial stage where the surface morphology has not grown rough enough. There-

fore, the evolution from an initial smooth surface to the later rough morphology may exhibit transient layer-by-layer growth behavior. In this section, we shall study in detail the diffraction aspects related to the transient layer-by-layer process.

##### A. General diffraction form: Damped oscillatory Bragg intensity

Similar to the diffraction line shape for a two-level system shown in Sec. III, the diffraction structure factor during growth can be divided into two parts. One is a sharp central  $\delta$  function associated with the long-range behavior in a surface. Another has a broad diffuse component and is related to short-range properties. The 2D Lorentzian function shown in Eq. (14) is an example. Equation (13) can be rewritten as

$$S(\mathbf{k}_{\parallel}, k_{\perp}) = \int d\mathbf{r} C(\phi, \mathbf{r} \rightarrow \infty) e^{i(\mathbf{k}_{\parallel} - \mathbf{G}_{hk}) \cdot \mathbf{r}} + \int d\mathbf{r} \Delta C(\phi, \mathbf{r}) e^{i(\mathbf{k}_{\parallel} - \mathbf{G}_{hk}) \cdot \mathbf{r}} \sim C(\phi, \mathbf{r} \rightarrow \infty) \delta(\mathbf{k}_{\parallel} - \mathbf{G}_{hk}) + S_{\text{diff}}(\mathbf{k}_{\parallel}, k_{\perp}), \quad (15)$$

where

$$\Delta C(\phi, \mathbf{r}) = C(\phi, \mathbf{r}) - C(\phi, \mathbf{r} \rightarrow \infty), \quad (16)$$

and the diffuse structure factor is given by

$$S_{\text{diff}}(\mathbf{k}_{\parallel}, k_{\perp}) = \int d\mathbf{r} \Delta C(\phi, \mathbf{r}) e^{i(\mathbf{k}_{\parallel} - \mathbf{G}_{hk}) \cdot \mathbf{r}}. \quad (17)$$

The  $\delta$  component in Eq. (15) corresponds to the Bragg peak intensity, which is proportional to  $C(\phi, \mathbf{r} \rightarrow \infty)$ . From the definition of the height difference function,  $C(\phi, \mathbf{r}) = \langle e^{i\phi[h(\mathbf{r}) - h(0)]} \rangle$ , we can obtain  $C(\phi, \mathbf{r} \rightarrow \infty)$  as

$$C(\phi, \mathbf{r} \rightarrow \infty) \approx \langle e^{i\phi h(\mathbf{r})} \rangle \langle e^{i\phi h(0)} \rangle = |\langle e^{i\phi h(0)} \rangle|^2, \quad (18)$$

where the derivation is based on the fact that, over a distance much larger than the lateral correlation length, the surface height fluctuations should not be correlated.

The calculation of the average phase factor  $\langle e^{i\phi h(0)} \rangle$  requires knowledge of the surface height distribution. In Sec. II, we have shown that for both MBE and surface-tension models, the height distribution at a late stage is represented rigorously by a Gaussian function shown in Eq. (5). The Gaussian distribution might not describe exactly the morphology for the growth of first several layers. However, for the subsequent growth, the Gaussian function should be a reasonable approximation when certain roughness has been built up. In addition, considering the discrete lattice effect for a crystalline surface, we have to employ a discrete height distribution instead of a continuous one. With a discrete Gaussian distribution, the calculation of  $\langle e^{i\phi h(0)} \rangle$  is straightforward. As shown in Appendix B, the result is given by Eq. (B5) as

$$\langle e^{i\phi h(0)} \rangle \approx e^{i\phi \langle h \rangle} [e^{-(1/2)[\phi]^2 (w/c)^2} + e^{\pm i 2\pi \langle h \rangle} e^{-(1/2)(2\pi - |\phi|)^2 (w/c)^2}],$$

where  $\langle h \rangle$  denotes  $\langle h(t) \rangle$  and  $[\phi]$  means  $\phi$  modulo  $2\pi$  such that  $-\pi \leq [\phi] \leq \pi$ .

The corresponding Bragg intensity or the  $\delta$  intensity ( $\propto |\langle e^{i\phi h(t)} \rangle|^2$ ) is given by

$$I_{\text{Bragg}}(\phi) \propto e^{-[\phi]^2(w/c)^2} + e^{-(2\pi - |[\phi]|)^2(w/c)^2} + 2 \cos[2\pi \langle h(t) \rangle] e^{-(1/2)[\phi]^2(w/c)^2} \times e^{-(1/2)(2\pi - |[\phi]|)^2(w/c)^2}, \quad (19)$$

which is an oscillatory function of the film thickness,  $\langle h(t) \rangle$ . The oscillatory amplitude depends on  $e^{-(1/2)[\phi]^2(w/c)^2} e^{-(1/2)(2\pi - |[\phi]|)^2(w/c)^2}$ , a Debye-Waller-like factor which is very sensitive to  $w$ . Since the interface width increases due to the roughening evolution during growth, as shown in Eqs. (4) and (8), the oscillatory amplitude must decay with time until it finally vanishes. Therefore, the Bragg intensity shown in Eq. (19) exhibits a damped oscillation, which reflects the transition from the layer-by-layer to multilayer growth.

The Bragg intensity in Eq. (19) also depends on the diffraction condition,  $\phi = k_{\perp}c$ . At out-of-phase conditions, one has

$$I_{\text{Bragg}}(\pi) \propto e^{-\pi^2(w/c)^2} [1 + \cos(2\pi \langle h(t) \rangle)]. \quad (20)$$

$$\left\langle \sin \left[ \frac{2\pi Z(\mathbf{r}, t)}{c} \right] \right\rangle = \frac{1}{\sqrt{2\pi w}} \int_{-\infty}^{+\infty} dZ \exp \left[ -\frac{[Z - \langle Z(t) \rangle]^2}{2w^2} \right] \sin \left[ \frac{2\pi Z}{c} \right] = e^{-Aw^2} \sin[2\pi \langle h(t) \rangle],$$

where  $\langle h(t) \rangle = \langle Z(t) \rangle / c$  and  $A = 2(\pi/c)^2$ . The growth rate equation (3) is then simplified as

$$\frac{\partial}{\partial t} \langle h(t) \rangle = R_0 - Y_0 e^{-Aw^2} \sin[2\pi \langle h(t) \rangle], \quad (21)$$

where  $R_0 = (D\Delta\mu/T)/c$  and  $Y_0 = V/c$ . Note that Eq. (21) works only when the driving force is large enough so that  $R_0 > Y_0$ .

To solve Eq. (21), we treat the interface width  $w$  as a constant based on the fact that  $w$  is a slowly varying function shown in Eq. (4),  $w^2 \sim \ln(1 + t/\tau_c)$ , as compared with the quick oscillatory function  $\sin(2\pi \langle h(t) \rangle)$  during layer-by-layer repetitions. (Actually, the interface width  $w$  should also be modulated by the layer repetitions due to the intrinsic substrate effect, as pointed out in Refs. 28 and 34. However, under the present approximation, in which we have assumed that the effect is less significant, we ignore such small modulations). Under the condition of  $R_0 > Y_0$ , from Eq. (21) we obtain a solution which shows an oscillatory growth rate

$$R(t) = \frac{\partial}{\partial t} \langle h(t) \rangle = \frac{R_0^2 - (Y_0 e^{-Aw^2})^2}{R_0 + Y_0 e^{-Aw^2} \sin[\omega(t + t_0) + \Phi]}, \quad (22)$$

where  $\omega = 2\pi \sqrt{R_0^2 - (Y_0 e^{-Aw^2})^2}$ ,  $\tan(\Phi) = Y_0 e^{-Aw^2} / \sqrt{R_0^2 - (Y_0 e^{-Aw^2})^2}$ , and  $t_0$  is a constant determined by

Both the oscillation and the intensity decay originate from the destructive interference of the diffraction from a surface having more than two levels. For a film with a thickness of a half-integer number of monolayers,  $\langle h(t) \rangle = m + \frac{1}{2}$ , the Bragg intensity vanishes, similar to that in an ideal layer-by-layer growth process, shown in Fig. 3(a). Note that Eq. (19) does not hold at the exact in-phase condition  $\phi = 2n\pi$ , where a rigorous expression gives  $|\langle e^{i2n\pi h(t)} \rangle|^2 = 1$  (see Appendix B). At  $\phi = 2n\pi$ , the intensity neither oscillates nor decays because of the constructive interference between different layers of atoms. An example for this in-phase diffraction condition is shown in Fig. 5(a).

### B. Diffraction from transient layer-by-layer growth: Surface-tension model

For the surface-tension model, the characteristics of the transient layer-by-layer growth at the initial stage can be demonstrated by a simple mean-field analysis from the growth rate equation (3). Using the Gaussian distribution of Eq. (5) as a mean-field approach, we are able to carry out the average of the pinning force in Eq. (3) as

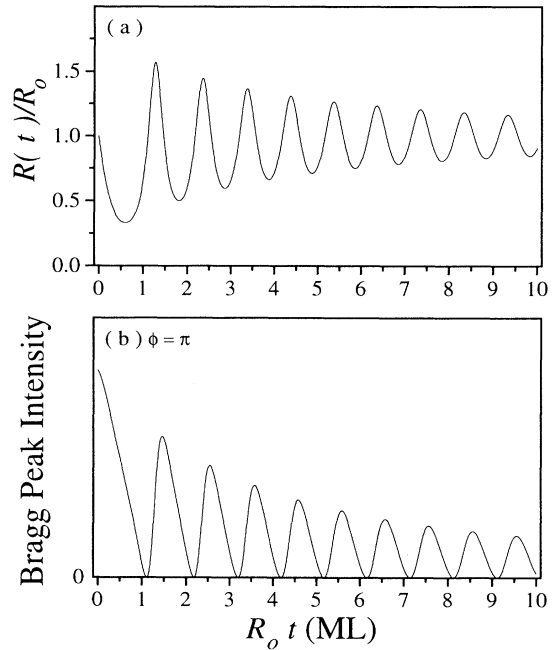


FIG. 4. (a) The growth rate  $R(t)$  is plotted against the deposition flux  $R_0 t$ , as calculated according to the surface-tension model. The oscillation is originated from the evaporation and condensation processes during growth. (b) The corresponding Bragg peak intensity as a function of  $R_0 t$ . The intensity oscillation decays in a form of power law,  $(1 + t/\tau_c)^{-\gamma}$ .

the initial condition. In Fig. 4(a), we plot  $R(t)$  as a function of the deposition flux,  $R_0 t$ , where  $w^2 \propto \ln(1+t/\tau_c)$  is given by Eq. (4). The growth rate  $R(t)$  shows a damped oscillation, which originates from evaporation and condensation during growth, as discussed in Sec. II. Since the oscillatory amplitude  $\propto Y_0 e^{-Aw^2}$ , it decays when the interface width increases. When the surface grows rough enough so that  $Y_0 e^{-Aw^2} \rightarrow 0$ , the oscillation disappears and  $R(t) \rightarrow R_0$ . The growth-induced roughening eventually evolves into the late stage of dynamic scaling region.

The factor  $\cos[2\pi\langle h(t)\rangle]$  in Eq. (19) can be calculated directly from the growth rate equations (21) and (22), i.e.,

$$I_{\text{Bragg}}(\pi) \propto (1+t/\tau_c)^{-\gamma} \left\{ 1 + \frac{\sqrt{R_0^2 - Y_0^2(1+t/\tau_c)^{-2\gamma}} \cos[\omega(t+t_0) + \Phi]}{R_0 + Y_0(1+t/\tau_c)^{-\gamma} \sin[\omega(t+t_0) + \Phi]} \right\}, \quad (23)$$

where  $\gamma$  is a constant. To show the damped oscillation, in Fig. 4(b) we plot the Bragg intensity of Eq. (23) as a function of the deposition flux,  $R_0 t$ . As shown in Fig. 4(b), the oscillatory intensity decays with time as a power law,  $(1+t/\tau_c)^{-\gamma}$ .

We also note that the minimal positions where the Bragg intensity vanishes do not occur at the half-integers of  $R_0 t$ . Recall that the Bragg intensity vanishes when the film thickness reaches a half-integer of monolayers,  $\langle h(t)\rangle = m + \frac{1}{2}$ , as shown in Eq. (20). In Fig. 4(b), the first minimal position occurs at  $R_0 t \approx 1.1$  ML. This implies that with a total of 1.1-ML materials being deposited on the surface, only a half-ML of the material sticks on the substrate while the rest of it simply evaporates. Starting from a flat substrate, the 2D nucleation in the first layer is difficult, which leads to a delay of the first minimal position occurring in the intensity oscillation shown in Fig. 3(b). However, when the film grows thicker and rougher, a growing number of steps and kinks are created to provide more sites which are energetically favorable for nucleation. Accordingly, the growth becomes easier. As shown in Fig. 4(b), at  $R_0 t > 3$  ML, i.e., after growth of the first several layers, the interval between nearest minimal positions are roughly equal to 1. This indicates that the average growth rate over each oscillation period is approximately equal to the impinging rate,  $R_0$ , although the oscillation of the growth rate still exists as shown in Fig. 4(a). We point out that the delay of the first monolayer growth has been observed in many experiments.<sup>4,25,34,49</sup> Although several possible explanations were given, our present result provides a physical approach for this phenomenon.

### C. Diffraction from transient layer-by-layer growth: Conservative MBE growth

For a conservative MBE growth, the growth rate is exactly equal to the impinging rate of deposition,  $\partial/\partial t \langle Z(\mathbf{r}, t)\rangle = R$ , which is in contrast to that for the nonconservative surface tension model, where  $\partial/\partial t \langle Z(\mathbf{r}, t)\rangle \neq R$ , due to the evaporation and reconden-

$\cos[2\pi\langle h(t)\rangle]$

$$= \frac{\sqrt{R_0^2 - (Y_0 e^{-Aw^2})^2} \cos[\omega(t+t_0) + \Phi]}{R_0 + Y_0 e^{-Aw^2} \sin[\omega(t+t_0) + \Phi]}.$$

Using this oscillatory factor and the interface width,  $w^2 \propto \ln(1+t/\tau_c)$ , we can calculate Eq. (19) for the present surface-tension growth model. At the out-of-phase diffraction condition  $[\phi] = \pi$ , the Bragg intensity is given by

sation processes. For a conservative MBE process, the film thickness increases linearly with time as

$$\langle h(t)\rangle = \langle Z(\mathbf{r}, t)\rangle / c = Rt / c.$$

In addition, the interface width can be approximately represented by  $w = \sqrt{A_0 t^{1/4}}$ , according to Eq. (8), where  $A_0$  is a constant. Inserting both  $w$  and  $\langle h(t)\rangle$  into Eq. (19), we obtain the Bragg intensity for an initial MBE growth process:

$$I_{\text{Bragg}}(\phi) \propto e^{-A_0[\phi]^2 t^{1/2}} + e^{-A_0(2\pi - |\phi|)^2 t^{1/2}} + 2 \cos(2\pi Rt/c) e^{-A_0[\phi]^2 t^{1/2}} \times e^{-A_0(2\pi - |\phi|)^2 t^{1/2}}. \quad (24)$$

To show the damped oscillatory behavior, in Fig. 5(b) we plot the Bragg intensity of Eq. (24) as a function of the growth time  $t$  at exactly the out-of-phase condition,  $\phi = k_1 c = \pi$ . As shown in Fig. 5(b), the intensity oscillation decays exponentially as  $e^{-2A_0\pi^2 t^{1/2}}$ , which is in contrast to the surface-tension model, where the oscillatory intensity decays with time as a power law,  $(1+t/\tau_c)^{-\gamma}$ , shown in Fig. 4(b). For a comparison, in Fig. 5(c) we also plot the Bragg intensity at  $\phi = k_1 c = 0.5\pi$ , which corresponds to a diffraction condition that has been frequently used in x-ray-diffraction and RHEED techniques. It is shown in Fig. 5(b) that the minimal intensity of the oscillation reaches zero because of the complete destructive interference at out-of-phase conditions. This does not occur at  $\phi = 0.5\pi$  due to the partial destructive interference, as shown in Fig. 5(c). These results are compared with Fig. 5(a), which shows the corresponding plot at the in-phase condition,  $k_1 c = 2\pi$ . In this case, the Bragg intensity neither oscillates nor decays due to constructive interference from different levels of atoms.

### D. Diffuse line shape

The calculation of the diffuse intensity is much more complicated. We shall give only a qualitative description

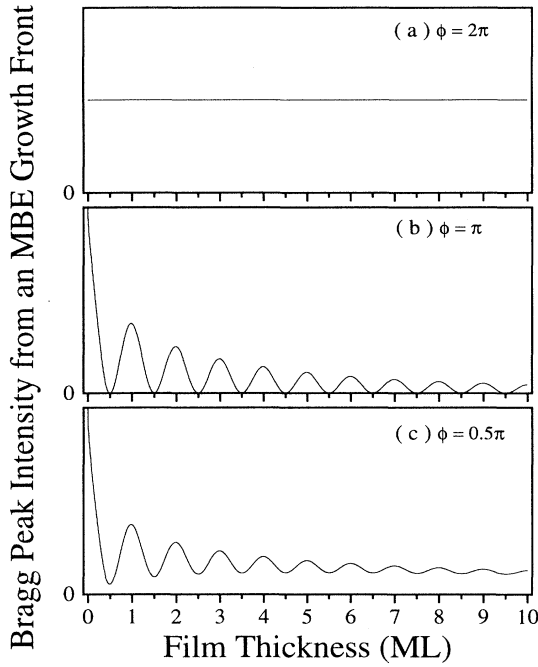


FIG. 5. The Bragg peak intensity as a function of film thickness is plotted at (a)  $\phi = 2\pi$  (in-phase condition), (b)  $\phi = \pi$  (out-of-phase condition), and (c)  $\phi = 0.5\pi$ . The intensity is calculated according to the conservative MBE model. Note that in (b), the intensity oscillation decays exponentially as  $e^{-2A_0\pi^2t^{1/2}}$ .

without going through a detailed derivation.

For the initial growth of first several layers, where the surface is still flat, the diffuse line shape is expected to be similar to a 2D Lorentzian function as shown in Eq. (14) in Sec. III. The FWHM of the Lorentzian line shape ( $\propto \xi^{-1}$ ) does not depend on the diffraction condition  $[\phi]$ . On the other hand, after a sufficiently long time, where the growth is in the late stage of roughening evolution showing dynamic scaling, the diffuse structure factor shown in Eq. (17) can be calculated from the height-height correlation function according to the relationship<sup>52</sup>

$$\begin{aligned} \Delta C(\phi, \mathbf{r}) &= C(\phi, \mathbf{r}) - C(\phi, \mathbf{r} \rightarrow \infty) \\ &\approx e^{-(1/2)[\phi]^2 \langle [h(\mathbf{r}) - h(0)]^2 \rangle} \end{aligned}$$

For the surface-tension growth model in which the height-height correlation is given by Eq. (6), we obtain a power-law function  $\Delta C(\phi, \mathbf{r}) \sim r^{-\chi(\phi)}$ , where  $\chi(\phi) \propto [\phi]^2$ . Therefore, at the later stage, the diffuse profile has a power-law tail shape given by

$$S_{\text{diff}}(\mathbf{k}_{\parallel}, k_{\perp}) = \int d\mathbf{r} \Delta C(\phi, \mathbf{r}) e^{i\mathbf{k}_{\parallel} \cdot \mathbf{r}} \sim k_{\parallel}^{-2+\chi(\phi)} (k_{\parallel} > \xi^{-1}), \quad (25)$$

which is similar to that for the equilibrium KT rough surface. We thus expect that, for the surface-tension growth model, the diffuse line shape should transform from a 2D Lorentzian function to a power-law function

when the growth proceeds from the initial stage of transient layer-by-layer fashion to the late stage of roughening evolution.

For the MBE growth model, the diffuse line shape does not have an analytical form. However, it has been shown<sup>50-52</sup> rigorously that for a scale-invariant surface structure described by  $\langle [h(\mathbf{r}) - h(0)]^2 \rangle \sim (r/L)^{2\alpha}$  ( $\alpha > 0$ ), the corresponding diffuse line shape is given by

$$S_{\text{diff}}(\mathbf{k}_{\parallel}, k_{\perp}) \sim ([\phi]^{-1/\alpha} L)^2 F_{\alpha}(k_{\parallel} |[\phi]|^{-1/\alpha} L),$$

where  $F_{\alpha}(x) = \int_0^{\infty} y dy e^{-y^{2\alpha}} J_0(xy)$ , and  $L$  is the average terrace width in the rough surface. This formula exhibits two power-law relationships in the reciprocal space, i.e., the peak intensity  $S_{\text{diff}}(\mathbf{k}_{\parallel} = 0, k_{\perp}) \sim |[\phi]|^{-2/\alpha}$  and the width of the profile:  $\text{FWHM} \sim |[\phi]|^{1/\alpha}$ . We therefore expect that as the growth proceeds from the initial stage of transient layer-by-layer fashion to the late stage of roughening evolution, the relationship of FWHM vs  $[\phi]$  for the diffuse line shape should transform from a constant to a power-law function.

#### V. COMPARISON WITH A MBE EXPERIMENT: Si/Si(111) GROWTH

We have studied *in situ* low-temperature MBE growth of Si on a singular Si(111) surface<sup>39</sup> using the high-resolution low-energy electron-diffraction (HRLEED) technique.<sup>53</sup> We observed that a roughening evolution with dynamic scaling characteristics occurs at a late stage of growth under a deposition rate of  $8 \pm 1$  bilayers/min and a low temperature of  $275 \pm 5^\circ\text{C}$  (Si melting temperature is  $1410^\circ\text{C}$ ). An initial transient layer-by-layer growth was observed before the occurrence of late stage roughening evolution. In this section, we shall analyze the HRLEED line shapes obtained from the initial transient layer-by-layer process using the diffraction model (MBE model) developed in Sec. IV B.

The experiment was performed in an UHV chamber equipped with a HRLEED system<sup>53</sup> and a Si evaporator.<sup>54</sup> The detailed description of the growth experiment has been described in Ref. 39. The steps in Si(111) surfaces created during deposition are biatomic (bilayer) steps as determined from out-of-phase diffraction conditions of HRLEED. At a sample temperature of  $275 \pm 5^\circ\text{C}$  and under a deposition rate of  $8 \pm 1$  bilayers/min, the growth of Si/Si(111) was monitored by HRLEED. Figure 6 shows the time-dependent line shapes of the (00) beam intensity scanned along the  $[\bar{1}\bar{1}2]$  direction. The data were taken at an electron-beam energy  $E = 47$  eV corresponding to an out-of-phase condition  $\phi = k_{\perp}c \approx 7.0\pi$ , where  $c = 3.135 \text{ \AA}$  is the bilayer step height for the Si(111) surface.

As shown in Fig. 6, at  $t = 0$  (before deposition), the line shape exhibits a sharp  $\delta$ -like profile that is identical to the HRLEED instrument response (a Gaussian shape function). The initial Si(111) substrate that we used was therefore step free within the instrument resolution. (The instrument can resolve a terrace width of at least  $1000 \text{ \AA}$ ). Once the deposition proceeds, a diffuse profile builds up and superimposes to the central  $\delta$  component,

as demonstrated in Fig. 6 for  $t > 0$ . Such a  $\delta$  diffuse line shape agrees with the diffraction theory developed in Sec. IV A. A further analysis indicates that the diffuse line shape is consistent with a 2D Lorentzian type of function, as described by Eq. (14) in Sec. III. The convolution of  $\delta + L_2$  with the instrument response (a Gaussian function) leads to a line shape of a Gaussian superimposed on a convoluted Lorentzian:  $G + G * L_2$ . It was found that all line shapes shown in Fig. 6 can be fitted well by the  $G + G * L_2$  function, where the Gaussian intensity, the Lorentzian intensity, and the Lorentzian width are adjustable parameters. Such a decomposition of the line shape into  $G + G * L_2$  allows us to extract from the fits the value of the Gaussian intensity which is proportional to the Bragg peak intensity. In Fig. 7, the extracted Bragg peak intensity (solid circles) is plotted as a function of the deposition time, which exhibits damped oscillatory behavior.

As shown in Fig. 7, at  $t = 15$  s, the thickness of the growing film is about two bilayers and the Bragg intensity reaches a maximum. Recall that, for a two-level surface, the Lorentzian diffuse profile should completely vanish when the Bragg intensity reaches a maximum, as shown

in Eq. (14). (For the present case,  $\theta \approx 0$  and  $\langle h(t) \rangle \approx 2$  bilayers). The fact that the diffuse profile still exists at  $t = 15$  s, as shown in Fig. 6, is a clear indication that certain roughness has built up in the growing film and the corresponding morphology has more than two levels. However, the transient layer-by-layer growth can still exist. At  $t = 21$  s, where  $\langle h(t) \rangle \approx 2.5$  bilayers (see Fig. 7), the Bragg peak almost disappears (see Fig. 6), which is due to the complete destructive interference of the diffraction from the surface with nearly half-bilayer coverage. As the growth continues, the behaviors similar to that occurring at  $t = 15$  and 21 s were observed again, as shown in Fig. 6 at  $t = 24$  and 30 s, where  $\langle h(t) \rangle \approx 2.8$  and 3.5 bilayers, respectively. The repetition is further shown at  $t = 42$  and 48 s. Such repetitions clearly demonstrate the transient layer-by-layer growth at the initial stage.

As the growth proceeds further, the central  $\delta$  component is significantly reduced, as shown in Fig. 6 at  $t > 80$  s. Such a reduction can be also seen in the damped oscillation of the Bragg intensity shown in Fig. 7. The  $\delta$  component vanishes completely (not shown) at  $t = 3$  min, where the growing film evolves into the region of the dy-

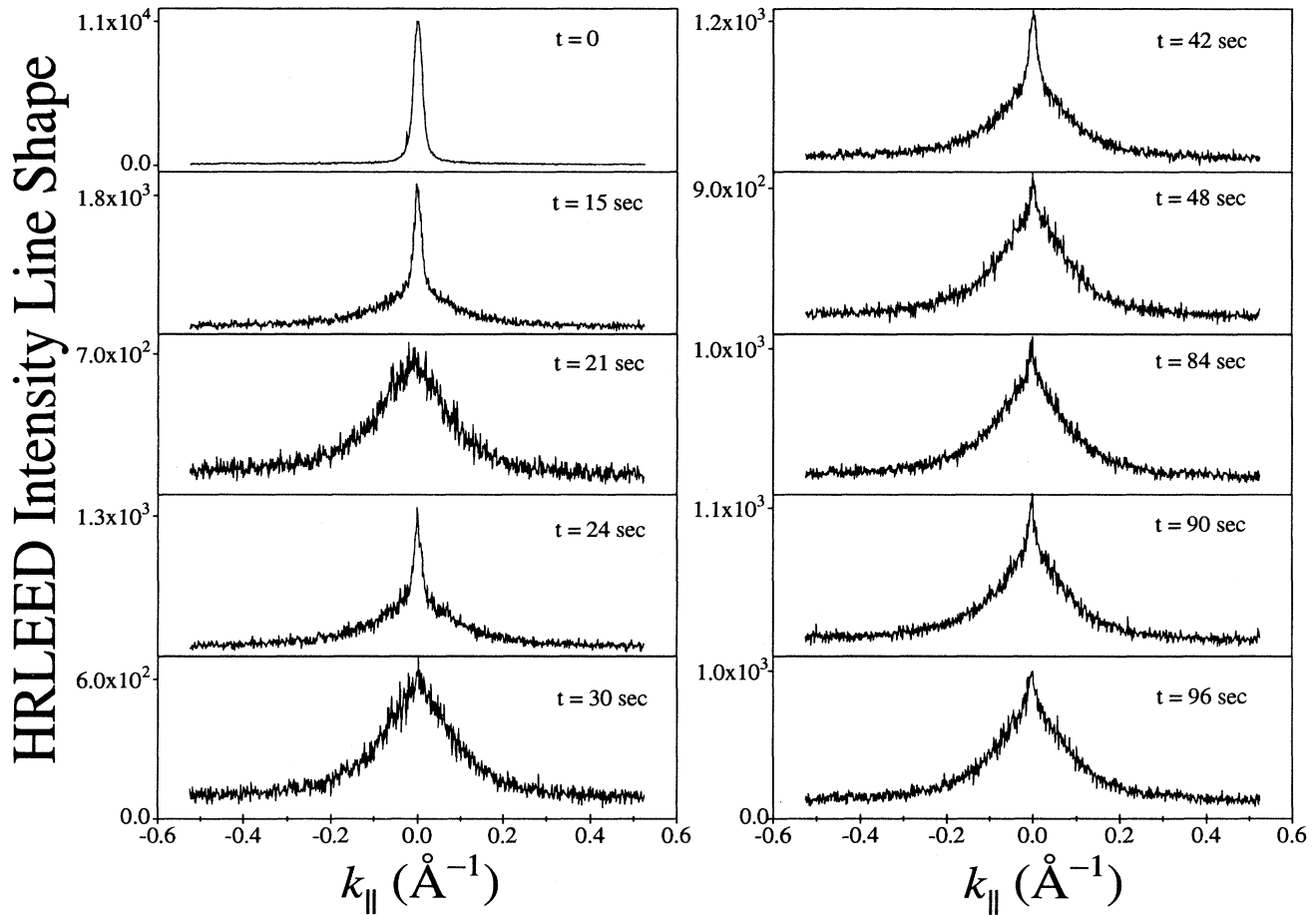


FIG. 6. The time-dependent HRLEED line shapes of the (00) beam intensity measured from an *in situ* MBE growth front, Si/Si(111). The intensity profiles were scanned along the  $[\bar{1}\bar{1}2]$  direction, and the data were taken at the electron-beam energy  $E = 47$  eV, corresponding to an out-of-phase condition,  $\phi = k_{\parallel}c \approx 7.0\pi$ .

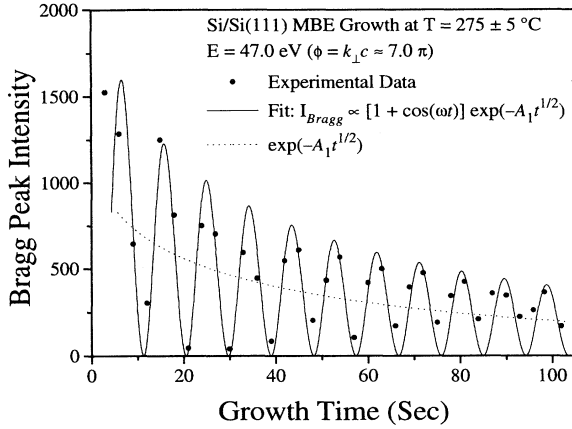


FIG. 7. The time-dependent Bragg peak intensities are plotted as filled circles, which are extracted from the measured line shapes shown in Fig. 6. The observed damped intensity oscillation is consistent with the form,  $I_0[1 + \cos(\omega t)]e^{-A_1 t^{1/2}}$ , which is plotted as the solid curve. The dashed curve represents the plot of the corresponding damping factor,  $e^{-A_1 t^{1/2}}$ .

dynamic roughening and scaling.<sup>39</sup> We try to fit the experimental data (solid circles) in Fig. 7 using a form  $I_0[1 + \cos(\omega t)]e^{-A_1 t^{1/2}}$ , according to the MBE model shown in Eq. (24) for the out-of-phase condition, where  $I_0$ ,  $\omega$ , and  $A_1$  are adjustable parameters. The solid curve in Fig. 7 represents the fit, while the dashed curve is the plot of the corresponding damping factor,  $e^{-A_1 t^{1/2}}$ . It is shown that the fit is reasonably good, except at the very initial region,  $t < 5$  s, where the intensity form, Eq. (24), which is derived from a Gaussian height distribution, may not be valid, as we pointed out in Sec. IV A.

Note that we do not intend to fit the present data using the power-law type of intensity form, Eq. (23), derived from the surface-tension model. This is because our study has shown that at the late stage of growth, the dynamic scaling behavior for Si/Si(111) is described by the Wolf-Villain model (the conservative MBE model). We have found that during the growth of Si/Si(111), the

roughness exponent  $\alpha \approx 1$  and the growth exponent  $\beta \approx \frac{1}{4}$ . To describe the transient oscillatory behavior shown in Fig. 7, we should then use the intensity expression given by Eq. (24), which was developed based on the Wolf-Villain model. At the present time, we have no experimental data available to test Eq. (23) for the surface-tension model. However, one of the potential candidates is the growth of GaAs film, where evaporation-condensation processes were observed to occur and the late-stage scaling dynamics appears to be more consistent with the Edwards-Wilkinson model.<sup>37</sup>

## VI. SUMMARY

We have shown an analytical formulation for the diffraction from an initial transient layer-by-layer growth front. The approach utilizes recently developed dynamic scaling models which describe the growth-induced roughening evolution of the growth fronts. The derived Bragg peak intensity shows a damped oscillation with the oscillatory amplitude decaying with the increase of the interface width. The results can be applied to both the out-of-phase and non-out-of-phase diffraction conditions. The derived diffraction formula is consistent with the experimental data from a transient layer-by-layer process observed in low temperature MBE growth of Si/Si(111).

## ACKNOWLEDGMENT

This work was supported by the NSF under Grant No. 9213023.

## APPENDIX A: SOLUTION OF STOCHASTIC LINEAR LANGEVIN EQUATIONS

A general form for stochastic linear Langevin equations can be expressed as

$$\frac{\partial}{\partial t} Z(\mathbf{r}, t) = \nu \nabla^2 Z(\mathbf{r}, t) - \kappa \nabla^4 Z(\mathbf{r}, t) + R + \eta(\mathbf{r}, t), \quad (\text{A1})$$

where the case for  $\kappa=0$  is the Edwards-Wilkinson model, and  $\nu=0$  corresponds to the Wolf-Villain model. Assuming an initial condition  $Z(\mathbf{r}, t=0)=0$ , we can obtain an analytical solution for Eq. (A1) as

$$Z(\mathbf{r}, t) = \langle Z(t) \rangle + \frac{1}{2\pi} \int d\mathbf{q}_x d\mathbf{q}_y e^{i\mathbf{q} \cdot \mathbf{r}} \int_0^t d\tau \Theta(\mathbf{q}, \tau) e^{-(\nu q^2 + \kappa q^4)(t-\tau)}, \quad (\text{A2})$$

where  $\langle Z(t) \rangle = Rt$  represents the average film thickness and  $\Theta(\mathbf{q}, t)$  is the Fourier transform of the Gaussian random noise  $\eta(\mathbf{q}, t)$ ,

$$\Theta(\mathbf{q}, t) = \frac{1}{2\pi} \int dx dy \eta(\mathbf{r}, t) e^{-i\mathbf{q} \cdot \mathbf{r}}.$$

$\Theta(\mathbf{q}, t)$ 's are also independent Gaussian random variables,<sup>55</sup> which, according to Eq. (2), have the following relations:

$$\begin{aligned} \langle \Theta(\mathbf{q}, t) \rangle &= 0, \\ \langle \Theta(\mathbf{q}, t) \Theta(\mathbf{q}', t') \rangle &= 2D \delta(\mathbf{q} + \mathbf{q}') \delta(t - t'). \end{aligned} \quad (\text{A3})$$

To prove that Eq. (A2) is the solution for the stochastic linear Langevin equation, one can directly insert it into Eq. (A1) for examination.

Using Eqs. (A2) and (A3), we are able to calculate the interface width

$$\begin{aligned} w^2 &= \langle [Z(\mathbf{r}, t) - \langle Z(t) \rangle]^2 \rangle \\ &= D \int_0^{1/b_c} q dq \frac{1 - e^{-2(\nu q^2 + \kappa q^4)t}}{\nu q^2 + \kappa q^4}, \end{aligned} \quad (\text{A4})$$

and the height-height correlation function

$$\begin{aligned} & \langle [Z(\mathbf{r}, t) - Z(0, t)]^2 \rangle \\ & \propto D \int_0^{1/b_c} q dq [1 - J_0(qr)] \frac{1 - e^{-2(\nu q^2 + \kappa q^4)t}}{\nu q^2 + \kappa q^4}. \end{aligned} \quad (\text{A5})$$

For the Edwards-Wilkinson model where  $\kappa=0$ , Eqs. (A4) and (A5) recover Eqs. (4) and (6), respectively. In contrast, for the Wolf-Villain model where  $\nu=0$ , Eqs. (A4) and (A5) become Eqs. (8) and (9), respectively.

It can be seen from Eq. (A2) that  $Z(\mathbf{r}, t) - \langle Z(t) \rangle$  is the sum of a linear combination of the noise terms,  $\Theta(\mathbf{q}, t)$ , for different values of  $\mathbf{q}$  and  $t$ . Since  $\Theta(\mathbf{q}, t)$ 's are independent Gaussian random variables, one can conclude<sup>55</sup> that the stochastic variable  $Z(\mathbf{r}, t) - \langle Z(t) \rangle$  must obey a Gaussian distribution with the Gaussian width (standard deviation) given by Eq. (A4), i.e.,

$$\rho[Z - \langle Z(t) \rangle] = \frac{1}{\sqrt{2\pi w}} \exp \left[ -\frac{[Z - \langle Z(t) \rangle]^2}{2w^2} \right]. \quad (\text{A6})$$

We can further obtain an analytical expression for the interface width  $w$ . The expression for  $w^2$  shown in Eqs. (4) and (8) can be rewritten as

$$\begin{aligned} w^2 & \sim \int_0^{1/b_c} dq \frac{1 - e^{-(\xi q)^n}}{q^{n-1}} \\ & \approx \int_0^\infty dq \frac{1 - e^{-(\xi q)^n}}{q^{n-1}} e^{-(b_c q)^n}, \end{aligned} \quad (\text{A7})$$

where  $n=2$  corresponds to the Edwards-Wilkinson model in which the lateral correlation length  $\xi = \sqrt{2\nu t}$ , and  $n=4$  corresponds to the Wolf-Villain model with the lateral correlation length  $\xi = (2\kappa t)^{1/4}$ . The last step in Eq. (A7) is an approximation in which the effect of the short-wavelength cutoff  $1/b_c$  in the integral is replaced by a Gaussian cutoff  $e^{-(b_c q)^n}$ .

Let  $a = b_c^n$  and  $s = \xi^n + b_c^n$ . Equation (A7) becomes

$$w^2 \sim \int_0^\infty dq \frac{e^{-aq^n} - e^{-sq^n}}{q^{n-1}} = g(n, s). \quad (\text{A7}')$$

In order to calculate  $g(n, s)$ , we first differentiate  $g(n, s)$  with respect to  $s$ ,

$$\frac{\partial}{\partial s} g(n, s) = \int_0^\infty q dq e^{-sq^n} = C_n s^{-2/n},$$

$$\begin{aligned} \langle e^{i\phi h(0)} \rangle & = N^{-1} \int_{-\infty}^{+\infty} dx e^{-(x - \langle h \rangle)^2 / 2(w/c)^2} e^{ix\phi} \sum_{m=-\infty}^{+\infty} \delta(x - m) \\ & = N^{-1} \sum_{n=-\infty}^{+\infty} \int_{-\infty}^{+\infty} dx e^{-(x - \langle h \rangle)^2 / 2(w/c)^2} e^{ix(\phi + 2n\pi)} \\ & = (w/c) \sqrt{2\pi} N^{-1} \sum_{n=-\infty}^{+\infty} e^{-\frac{1}{2}(\phi + 2n\pi)^2 (w/c)^2} e^{i(\phi + 2n\pi)\langle h \rangle}. \end{aligned}$$

Similarly, the normalization constant is given by

$$N = (w/c) \sqrt{2\pi} \sum_{n=-\infty}^{+\infty} e^{-1/2(2n\pi)^2 (w/c)^2} e^{i2n\pi\langle h \rangle}.$$

where  $C_n$  is a constant,  $C_n = \int_0^\infty x dx e^{-x^n} = n^{-1} \Gamma(2/n)$ . We then reintegrate  $(\partial/\partial s)g(n, s)$  as

$$\begin{aligned} g(n, s) & = \int_a^s ds \frac{\partial}{\partial s} g(n, s) \\ & = C_n \int_a^s ds s^{-2/n} \propto \begin{cases} \ln(s/a) & \text{for } n=2 \\ s^{1/2} - a^{1/2} & \text{for } n=4. \end{cases} \end{aligned}$$

Inserting  $a = b_c^n$  and  $s = \xi^n + b_c^n$ , we conclude from Eq. (A7') that

$$w^2 \sim \begin{cases} \ln(1 + t/\tau_c) & \text{for the Edwards-Wilkinson model} \\ \sqrt{1 + t/\tau_c} - 1 & \text{for the Wolf-Villain model,} \end{cases} \quad (\text{A8})$$

where, for the Edwards-Wilkinson model,  $\tau_c = b_c^2/2\nu$ , and for the Wolf-Villain model  $\tau_c = b_c^4/2\kappa$ . Considering only the asymptotic behavior at the late stage,  $t \gg \tau_c$ , we have

$$w^2 \sim \begin{cases} \ln(t) & \text{for the Edwards-Wilkinson model} \\ t^{1/2} & \text{for the Wolf-Villain model.} \end{cases} \quad (\text{A9})$$

## APPENDIX B: CALCULATION OF $\langle e^{i\phi h(0)} \rangle$

For a crystalline surface, the surface height must be equal to integer numbers of the layer spacing  $c$ , i.e.,  $h(\mathbf{r}) = Z(\mathbf{r})/c = 0, \pm 1, \pm 2, \dots$ . Given a Gaussian height distribution shown in Eq. (5) for a crystalline surface,  $\langle e^{i\phi h(0)} \rangle$  can be calculated as

$$\langle e^{i\phi h(0)} \rangle = N^{-1} \sum_{m=-\infty}^{+\infty} e^{-(m - \langle h \rangle)^2 / 2(w/c)^2} e^{im\phi}, \quad (\text{B1})$$

where  $\langle h \rangle c = \langle Z \rangle$  is the average height and  $N$  is the normalization constant,

$$N = \sum_{m=-\infty}^{+\infty} e^{-(m - \langle h \rangle)^2 / 2(w/c)^2}. \quad (\text{B2})$$

In order to calculate the summation in Eq. (B1), we employ an identity

$$F(x) = \sum_{m=-\infty}^{+\infty} \delta(x - m) = \sum_{n=-\infty}^{+\infty} e^{i2n\pi x}, \quad (\text{B3})$$

where  $F(x)$  is a one-dimensional lattice function. Using Eq. (B2), we can calculate Eq. (B1) as

Thus a rigorous expression for  $\langle e^{i\phi h(0)} \rangle$  is given by

$$\langle e^{i\phi h(0)} \rangle = \frac{\sum_{n=-\infty}^{+\infty} e^{-1/2(\phi+2n\pi)^2(w/c)^2} e^{i(\phi+2n\pi)\langle h \rangle}}{\sum_{n=-\infty}^{+\infty} e^{-1/2(2n\pi)^2(w/c)^2} e^{i2n\pi\langle h \rangle}}. \quad (\text{B4})$$

For any in-phase condition  $\phi=2m\pi$ , we have  $\langle e^{i\phi h(0)} \rangle=1$  from Eq. (B4). For diffraction away from the in-phase condition, we can simplify Eq. (B4). It is shown that if  $(w/c) > 0.8$ ,  $e^{-(1/2)(2n\pi)^2(w/c)^2} \sim 0$  for any  $n \neq 0$ , and

$$\sum_{n=-\infty}^{+\infty} e^{-1/2(2n\pi)^2(w/c)^2} e^{i2n\pi\langle h \rangle} \approx 1.$$

Therefore, we can simplify Eq. (B4) to give

$$\begin{aligned} \langle e^{i\phi h(0)} \rangle &\approx \sum_{n=-\infty}^{+\infty} e^{-1/2(\phi+2n\pi)^2(w/c)^2} e^{i(\phi+2n\pi)\langle h \rangle} \\ &\approx e^{i\phi\langle h \rangle} [e^{-1/2[\phi]^2(w/c)^2} + e^{\pm i2\pi\langle h \rangle} e^{-1/2(2\pi-|\phi|)^2(w/c)^2}], \end{aligned} \quad (\text{B5})$$

where we only keep the first two terms in the summation.

- <sup>1</sup>E. Bauer, Z. Kristallogr. **110**, 372 (1958).  
<sup>2</sup>R. Kern, G. Le Lay, and J. J. Metois, *Basis Mechanisms in the Early Stages of Epitaxy*, Current Topics in Material Science Vol. 3 (North-Holland, Amsterdam, 1979), p. 131.  
<sup>3</sup>J. A. Venables, G. D. T. Spiller, and M. Hanbuchen, Rep. Prog. Phys. **47**, 399 (1984).  
<sup>4</sup>For a review, see *Reflection High-Energy Electron Diffraction and Reflection Electron Imaging of Surfaces*, edited by P. K. Larson and P. J. Dobson (Plenum, New York, 1988), and references therein.  
<sup>5</sup>E. Vlieg, A. W. Denier van der Gon, J. F. van der Veen, J. E. Macdonald, and C. Norris, Phys. Rev. Lett. **61**, 2241 (1988).  
<sup>6</sup>R. Kunkel, B. Poelsema, L. K. Verheij, and G. Comsa, Phys. Rev. Lett. **65**, 733 (1990).  
<sup>7</sup>B. G. Orr, J. Sudijono, and M. D. Johnson, in *Common Themes and Mechanisms of Epitaxial Growth*, edited by P. Fuoss, J. Tsao, D. W. Kisker, A. Zangwill, and T. Kuech, MRS Symposia Proceedings No. 312 (Materials Research Society, Pittsburgh, 1994), p. 15.  
<sup>8</sup>W. van Saarloos and G. H. Gilmer, Phys. Rev. B **33**, 4927 (1986).  
<sup>9</sup>S. T. Chui and J. D. Weeks, Phys. Rev. Lett. **40**, 733 (1978).  
<sup>10</sup>S. F. Edwards and D. R. Wilkinson, Proc. R. Soc. London Ser. A **381**, 17 (1982).  
<sup>11</sup>P. Nozières and F. Gallet, J. Phys. (Paris) **48**, 353 (1987).  
<sup>12</sup>P. Nozières, in *Solids Far From Equilibrium*, edited by C. Godriche (Cambridge University Press, New York, 1991), pp. 135–143.  
<sup>13</sup>D. E. Wolf and J. Villain, Europhys. Lett. **13**, 389 (1990).  
<sup>14</sup>Z.-W. Lai and S. Das Sarma, Phys. Rev. Lett. **66**, 2348 (1991); S. Das Sarma and S. V. Ghaisas, *ibid.* **69**, 3762 (1992); S. Das Sarma, S. V. Ghaisas, and J. M. Kim, Phys. Rev. E **49**, 122 (1993).  
<sup>15</sup>L.-H. Tang and T. Nattermann, Phys. Rev. Lett. **66**, 2899 (1991).  
<sup>16</sup>A. Zangwill, D. D. Vvedensky, C. N. Luse, and M. R. Wilby, Surf. Sci. **274**, L529 (1992); Phys. Rev. E **48**, 852 (1993).  
<sup>17</sup>M. Siegert and M. Plischke, Phys. Rev. Lett. **68**, 2035 (1992).  
<sup>18</sup>J. G. Amar, P.-M. Lam, and F. Family, Phys. Rev. E **47**, 3242 (1993); J. G. Amar and F. Family, in *Mechanisms of Thin Film Evolution*, edited by S. M. Yalisove, C. V. Thompson, and D. J. Eaglesham, MRS Symposia Proceedings No 317 (Materials Research Society, Pittsburgh, 1994).  
<sup>19</sup>M. Schroeder, M. Siegert, D. E. Wolf, J. D. Shore, and M. Plischke, Europhys. Lett. **24**, 563 (1993).  
<sup>20</sup>J. M. Kim and S. Das Sarma, Phys. Rev. Lett. **72**, 2903 (1994).  
<sup>21</sup>J. Krug, Phys. Rev. Lett. **72**, 2907 (1994).  
<sup>22</sup>For reviews, see, F. Family, in *Fractals in Natural and Applied Sciences*, edited by M. M. Novak (Elsevier Science, North-Holland, 1994), p. A-41; also see, *Dynamics of Fractal Surfaces*, edited by F. Family and T. Vicsek (World Scientific, Singapore, 1990), and references therein.  
<sup>23</sup>A. Madhuker and S. V. Ghaisas, CRC Crit. Rev. Solid State Mater. Sci. **14**, 1 (1988).  
<sup>24</sup>S. Clarke and D. D. Vvedensky, Phys. Rev. Lett. **58**, 2235 (1987).  
<sup>25</sup>R. Altsinger, H. Busch, M. Horn, and M. Henzler, Surf. Sci. **200**, 235 (1987); M. Horn, U. Gotter, and M. Henzler, J. Vac. Sci. Technol. B **6**, 727 (1987).  
<sup>26</sup>P. I. Cohen, G. S. Petrich, P. R. Pukite, G. S. Whaley, and A. S. Arrott, Surf. Sci. **216**, 222 (1989).  
<sup>27</sup>A. Rockett, J. Vac. Sci. Technol. B **6**, 713 (1988).  
<sup>28</sup>J. Kertész and D. E. Wolf, J. Phys. A **21**, 747 (1988).  
<sup>29</sup>R. Kariotis and M. G. Lagally, Surf. Sci. **216**, 557 (1989).  
<sup>30</sup>J. W. Evans, Phys. Rev. B **39**, 5655 (1989); **43**, 3897 (1991); J. W. Evans, D. E. Sanders, P. A. Thiel, and A. E. DePristo, *ibid.* **41**, 5410 (1990).  
<sup>31</sup>W. F. Eggelhoff and I. Jacob, Phys. Rev. Lett. **62**, 921 (1989).  
<sup>32</sup>B. W. Dobson, Phys. Rev. B **36**, 1068 (1987).  
<sup>33</sup>S. Das Sarma, J. Vac. Sci. Technol. A **8**, 2714 (1990); I. K. Marmorosk and S. Das Sarma, Surf. Sci. Lett. **237**, L411 (1990).  
<sup>34</sup>H. C. Kang and J. W. Evans, Surf. Sci. **271**, 321 (1992).  
<sup>35</sup>J. M. Kosterlitz and D. J. Thouless, J. Phys. C **6**, 1181 (1973).  
<sup>36</sup>F. Gallet, S. Balibar, and E. Rolley, J. Phys. (Paris) **48**, 369 (1987).  
<sup>37</sup>M. K. Nissen, C. Lavoie, S. R. Johnson, J. A. Mackenzie, and T. Tiedje, Bull. Am. Phys. Soc. **39**, 333 (1994).  
<sup>38</sup>J. Krug, M. Plischke, and M. Siegert, Phys. Rev. Lett. **70**, 3271 (1993).  
<sup>39</sup>H.-N. Yang, G.-C. Wang, and T.-M. Lu, Phys. Rev. Lett. **73**, 2348 (1994).

- <sup>40</sup>C. S. Lent and P. I. Cohen, *Surf. Sci.* **139**, 121 (1984).
- <sup>41</sup>J. M. Pimbley and T.-M. Ju, *J. Vac. Sci. Technol. A* **2**, 457 (1984); *J. Appl. Phys.* **57**, 1121 (1985).
- <sup>42</sup>M. den Nijs and K. Rommelse, *Phys. Rev. B* **40**, 4709 (1989).
- <sup>43</sup>M. den Nijs, in *Phase Transition in Surface Films, 1990 Summer NATO Proceedings*, edited by H. Taub (Plenum, New York, 1990).
- <sup>44</sup>H.-N. Yang, K. Fang, T.-M. Lu, and G.-C. Wang, *Europhys. Lett.* **19**, 216 (1992).
- <sup>45</sup>M. Henzler, *Surf. Sci.* **73**, 240 (1978).
- <sup>46</sup>J. M. Pimbley and T.-M. Lu, *Surf. Sci.* **159**, 169 (1985).
- <sup>47</sup>K. Fang, H.-N. Yang, and G.-C. Wang, *Surf. Sci.* **284**, L399 (1993).
- <sup>48</sup>Q. Jiang, A. Chan, and G.-C. Wang, *Phys. Rev. B* **50**, 11 116 (1994).
- <sup>49</sup>R. Altsinger, H. Busch, M. Horn, and M. Henzler, *Surf. Sci.* **200**, 235 (1988).
- <sup>50</sup>Po-zen Wong and Alan J. Bray, *Phys. Rev. B* **37**, 7751 (1988).
- <sup>51</sup>S. K. Sinha, E. B. Sirota, S. Garoff, and H. B. Stanley, *Phys. Rev. B* **38**, 2297 (1988).
- <sup>52</sup>H.-N. Yang, T.-M. Lu, and G.-C. Wang, *Phys. Rev. Lett.* **68**, 2612 (1992); *Phys. Rev. B* **47**, 3911 (1993); *Diffraction From Rough Surfaces and Dynamic Growth Fronts* (World Scientific, Singapore, 1993).
- <sup>53</sup>U. Scheithauer, G. Meyer, and M. Henzler, *Surf. Sci.* **178**, 441 (1986); J.-K. Zuo, R. A. Harper, and G.-C. Wang, *Appl. Phys. Lett.* **51**, 250 (1987).
- <sup>54</sup>B. T. Jonker, *J. Vac. Technol. A* **8**, 383 (1990).
- <sup>55</sup>S.-K. Ma, *Statistical Mechanics* (World-Scientific, Singapore, 1985).